ANL/RERTR/TM-11-19

Estimation of Steady-State and Transient Power Distributions for the RELAP Analyses of the 1963 Loss-of-Flow and Loss-of-Pressure Tests at BR2

Nuclear Engineering Division

About Argonne National Laboratory
Argonne is a U.S. Department of Energy laboratory managed by UChicago Argonne, LLC under contract DE-AC02-06CH11357. The Laboratory's main facility is outside Chicago, at 9700 South Cass Avenue, Argonne, Illinois 60439. For information about Argonne and its pioneering science and technology programs, see www.anl.gov.

Availability of This Report
This report is available, at no cost, at http://www.osti.gov/bridge. It is also available on paper to the U.S. Department of Energy and its contractors, for a processing fee, from:

U.S. Department of Energy
Office of Scientific and Technical Information
P.O. Box 62
Oak Ridge, TN 37831-0062
phone (865) 576-8401
fax (865) 576-5728
reports@adonis.osti.gov

Disclaimer
This report was prepared as an account of work sponsored by an agency of the United States Government. Neither the United States Government nor any agency thereof, nor UChicago Argonne, LLC, nor any of their employees or officers, makes any warranty, express or implied, or assumes any legal liability or responsibility for the accuracy, completeness, or usefulness of any information, apparatus, product, or process disclosed, or represents that its use would not infringe privately owned rights. Reference herein to any specific commercial product, process, or service by trade name, trademark, manufacturer, or otherwise, does not necessarily constitute or imply its endorsement, recommendation, or favoring by the United States Government or any agency thereof. The views and opinions of document authors expressed herein do not necessarily state or reflect those of the United States Government or any agency thereof, Argonne National Laboratory, or UChicago Argonne, LLC.

ANL/RERTR/TM-11-19

Estimation of Steady-State and Transient Power Distributions for the RELAP Analyses of the 1963 Loss-of-Flow and Loss-of-Pressure Tests at BR2

by
B. Dionne and C.P. Tzanos
Nuclear Engineering Division, Argonne National Laboratory

May 23, 2011

This work is sponsored by the
U.S. Department of Energy, National Nuclear Safety Administration (NNSA)
Office of Global Threat Reduction (NA-21)

Table of Contents

1. Introduction 4
1.1. Background 4
1.2. Historical analysis 4
1.3. Scope of work 4
1.4. Report organization 5

2. BR2 reactor core description 5
2.1. Overview 5
2.2. Fuel characteristics 6
2.3. Core state during the loss-of-flow tests 6

3. Power calculation methodology for the 1963 tests 8
3.1. Codes descriptions 9
3.2. Overview of the methodology 9

4. Analyses performed during development of the methodology 17
4.1. Comparison of the ORIGEN-2 and ANS/ANSI 5.1 decay curves 17
4.2. Study of the time-dependency of the decay gamma spectrum 18
4.3. Criticality bias of the "configuration 4" MCNP model 21
4.4. Verification of the fuel assembly power predictions 21
4.5. Axial power distributions in current and historical approaches 22
4.6. Study of sector azimuthal peaking for test A 22
4.7. Change in the axial power profile during the transient 24

5. Computational results 24
5.1. Steady-state axial power in the instrumented sector for all tests 25
5.2. Steady-state power fraction for each region at initiation of test C 25
5.3. Steady-state axial power for regions during test A 26
5.4. Decay power for each region during test F 27
5.5. RELAP peak cladding temperature during test A 29

6. Conclusions 30

References 31

1. Introduction

1.1. Background

To support the safety analyses required for the conversion of the Belgian Reactor 2 (BR2) from highly-enriched uranium (HEU) to low-enriched uranium (LEU) fuel, the simulation of a number of loss-of-flow tests, with or without loss of pressure, has been undertaken. These tests were performed at BR2 in 1963 and used instrumented fuel assemblies (FAs) with thermocouples (TC) imbedded in the cladding as well as probes to measure the FAs power on the basis of their coolant temperature rise. The availability of experimental data for these tests offers an opportunity to better establish the credibility of the RELAP5-3D [1] model and methodology used in the conversion analysis.

1.2. Historical analysis

Past RELAP analysis of the test A [2] defined the instrumented FA power as the experimentally measured power during the test. The axial power distribution was taken from a BR02 mockup core flux distribution and adjusted to match the measured cladding temperatures at steady-state. All the remaining power needed to reach 24 MW was assumed deposited in the other FAs using the same axial profile. The ANS-1979 decay heat standard [3] was used to evaluate the decay power and point-kinetics was used evaluate the residual neutron power after scram. This approach has the advantage of reproducing exactly the measured cladding temperature at steady-state. However, used in a loss-of-flow transient, this approach appeared to significantly over-estimate the secondary clad temperature peak occurring near the moment of flow reversal.

1.3. Scope of work

Upon review of the historical approach, it was concluded that some improvements were needed for the following reasons:

- It cannot be easily applied to study any core configuration for which FA powers and cladding temperature measurements are not available.
- It provides only a crude spatial approximation of the power distribution (up to 5 points, i.e., based on the number of TC data available).
- It does not take into account that energy is transported from the fuel and deposited in adjacent structures.
- It does not take into account the change in the power spatial distribution following the reactor scram occurring during the transient.

Therefore, efforts were made to develop a methodology that would yield a steady-state power distribution for any core configuration and provide better estimates of the decay power distributions after scram. To obtain the power distributions for the instrumented FAs and the other regions of the core, an improved MCNP5 [4] model of the 1963 core configuration was developed from a previous model [5]. This model is used to obtain the

power distributions in the BR2 core during the tests. Decay power curves and decay gamma spectrum obtained from ORIGEN-2 [6] are used in conjunction with the MCNP model to estimate the power redistribution after reactor scram. This information is then used to automatically generate the RELAP steady-state and transient power cards.

The historical analysis used test A/400/1 (referred from here on as test A) as a benchmark case. Therefore some results presented in this work pertain to the analysis of this test. The same methodology is used for the analysis of two other loss-of-flow tests; test C/600/3 and test F/400/1 (referred from here on as test C and test F, respectively). When the results of the three tests will be similar, only a representative sample from a selected test will be shown.

1.4. Report organization

This report is organized as follows. Section 2 presents a short description of the BR2 including a description of the core state at the moment of each test. Section 3 describes in details the methodology and the assumptions used to estimate the steady-state and transient power distributions for use in the RELAP analyses. Section 4 presents results of some key analyses that were performed during the development of the methodology to evaluate the impact of model choices and verify the methodology. Section 5 presents the calculated power distributions used in the RELAP analyses of the tests. Finally, Section 6 summarizes and concludes the work presented in this report.

2. BR2 reactor core description

2.1. Overview

BR2 is a water-cooled reactor moderated by beryllium and water. The core, in a form of a twisted hyperboloid bundle, is located inside an aluminum pressure vessel. The beryllium consists of a matrix of hexagonal prisms, each with a central bore forming a channel. The flexibility of the BR2 core design allows for a variety of core loadings since each channel can contain one of the following: a control or regulating rod, an experimental device, a beryllium plug or a FA. Figure 1 shows a schematic of the reactor.

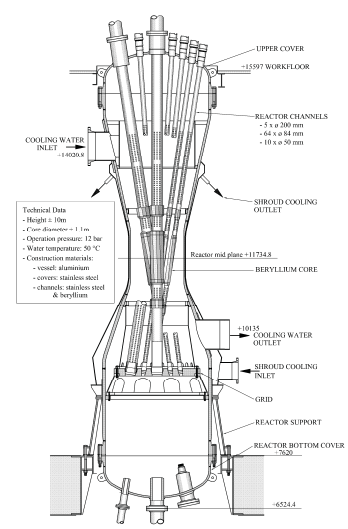

Figure 1. BR2 core schematic.

Figure 2 shows a section of the Sylcor VIa FA used in 1963. A Sylcor VIa BR2 FA is composed of six concentric fuel "tubes" divided by aluminum stiffeners into three sectors. Each fuel plate (sector) was composed of an UAl_x alloy meat clad by aluminum [7]. The central location of FA could

contain either an experimental device or a plug (Be or Al). The geometry of this type of FA is similar to FAs used in the current BR2 core.

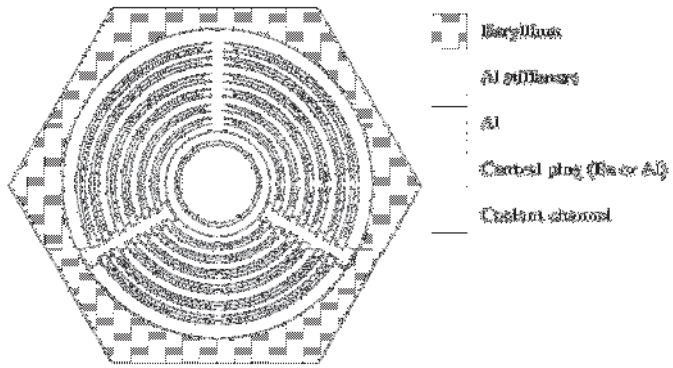

Figure 2. Section of a BR2 Sylcor VIa fuel assembly.

During the 1963 loss-of-flow tests, all the FAs had a central Be plug with the exception of the instrumented FAs which had an instrumented pin (power probe) [8, 9]. In this work, the instrumented pins are modeled as aluminum plugs. This approximation is justified since the pins should produce only a small perturbation to the flux profile beyond the water displacement (as modeled by the Al plug).

2.2. Fuel characteristics

The exact fuel meat composition of the Sylcor VIa FAs is not well defined in the available literature [7, 8, 9, 10]. It provides incomplete or inconsistent information for the following parameters; i) weight percent of uranium in the fuel meat, ii) porosity, iii) volume fraction of each component of UAl_x, and iv) exact enrichment. Therefore, Table 1 provides the fuel composition assumptions considered in this work.

Table 1. Assumptions about 1963 BR2 Sylcor VIa HEU fuel meat composition.

Assumption
UAl_x alloy
24 w/o of uranium in alloy (all UAl_4)
90% enriched in ^{235}U
244g of ^{235}U per assembly
~1 w/o ^{234}U, ~0.3 w/o of ^{236}U
1% porosity (typical for alloy)

2.3. Core state during the loss-of-flow tests

The loss-of-flow tests were performed about nine months after the BR2 startup. During that time, the reactor produced about 1850 MWd of energy [11]. Since an operating cycle

was dedicated to the tests, the core was loaded with 14 fresh FAs (4 of them instrumented) at the beginning-of-cycle (BOC). The core was also loaded with 7 control rods and 2 regulating rods in the arrangement (labeled as "configuration 4") shown in Fig. 3. Note that from herein on, BOC will refer to the beginning of the operating cycle dedicated to the tests.

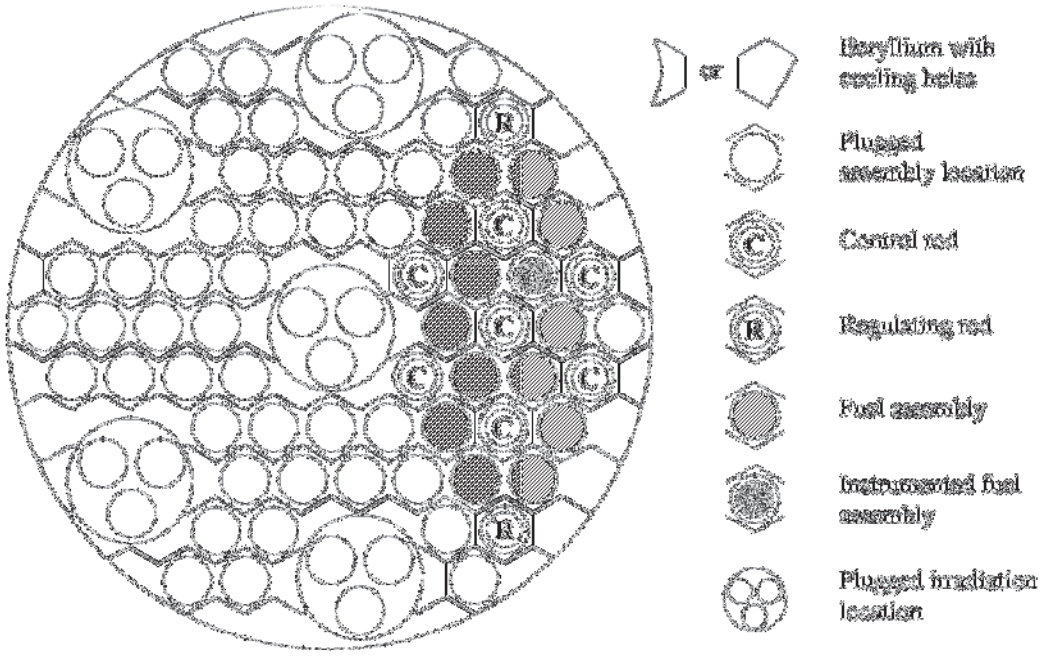

Figure 3. BR2 1963 core "configuration 4".

The four instrumented FAs had five thermocouples embedded in the azimuthal center of the outer cladding of the outermost plate as shown in Fig. 4.

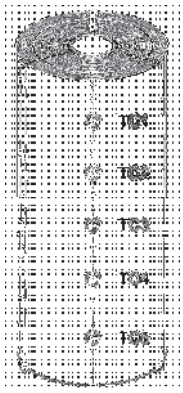

Figure 4. Locations of the thermocouples on an instrumented FA.

The thermocouple labeled TC13 was located at the axial mid-plane of the fuel meat, while the others were placed at ±150mm (TC12, TC14) and ±300 mm (TC11, TC15) from the mid-plane.

No information about the orientation of the FA within the core could be found in the documentation of the tests. Therefore, a reference orientation was selected arbitrarily based on the orientation illustrated in a drawing from Ref. 8.

Since no positions are provided in the operational log of the tests [11], the regulating rods are assumed to be nominally withdrawn to 250mm [12] at the initiation of all tests.

The detailed power history [11] from BOC to each test initiation is shown in Fig. 5.

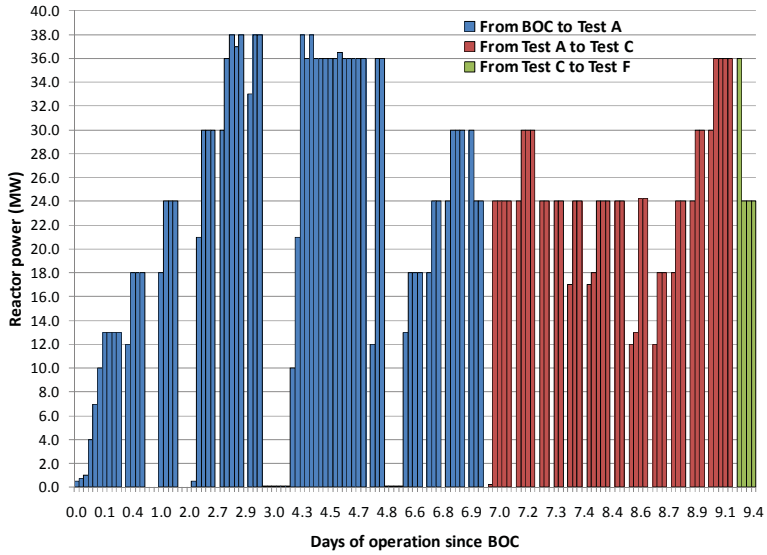

Figure 5. Detailed power history from BOC to the initiation of each test.

Table 2 gives other key parameters necessary to define the core state (from a reactor physics perspective) at the initiation of the tests.

Table 2. Key parameters defining the core state.

	At initiation of the test				
	Energy generated (MWd)	Days after BOC (days)	Reactor power (MW)	Maximum heat flux[1] (W/cm^2)	CR position[2] (mm)
Test A	54	7.0	24	400	551
Test C	103	9.1	36	600	593
Test F	110	9.4	24	400	640

[1] Based on original estimation performed in 1963
[2] CR position is quoted as the withdrawal height (0mm is fully inserted)

3. Power calculation methodology for the 1963 tests

The current methodology uses MCNP5 and ORIGEN-2. Therefore, brief descriptions of these two codes are provided in Section 3.1. The code used to predict the evolution of the beryllium matrix, BERYL [13], is also briefly described in that section. A discussion of each step of the methodology is presented in Section 3.2.

3.1. Codes descriptions

3.1.1. MCNP5

As used in this work, MCNP is a general-purpose Monte Carlo N-Particle code that allows for fixed source and criticality calculations taking into account the physics of neutrons and photons through ENDF-B/VII point-wise cross sections. For neutrons, all reactions given in a particular cross-section evaluation are accounted for. Thermal neutrons are described by both the free gas and S(α,β) models. The MCNP three-dimensional model of the reactor is defined by surfaces forming geometric cells to which materials are assigned. The MCNP energy deposition tallies for neutrons and photons, f6:n, f6:p and f6:n,p are used to obtain the three-dimensional profiles necessary to estimate the power distributions.

3.1.2. ORIGEN-2

ORIGEN is a point-depletion code designed to evaluate the buildup and decay of radioactive materials. Therefore, its main function is to calculate the time-dependent concentrations of nuclides using a matrix exponential method. It also evaluate the gamma source term associated with the fission products, actinides and other activated materials. ORIGEN-2 was the last version of the code to be distributed as a standalone version. It performs one-group depletion using ENDF/B-VI cross-sections libraries generated for spectra of different reactor systems. However, it allows the use of any cross-sections generated for other reactor systems.

3.1.3. BERYL

BERYL is a point-depletion code calculating the time-dependant (generation, depletion and decay) concentrations of the Be-9, Li-6, H-3 and He-3 isotopes for a given irradiation history of the beryllium matrix. This is performed by solving analytically a set of ordinary differential equations describing the proper simplified transmutation chains. Reactor-specific reaction rates must be provided (extracted from MCNP5 in this work) in addition to the power history.

3.2. Overview of the methodology

To obtain a better estimate of the steady-state and decay power distributions, the new methodology provides a detailed power distribution for each region of the core at steady-state and an estimate of the power redistribution during the transient for any core configuration. The methodology, illustrated in Fig. 6, is not significantly different from a typical Monte Carlo (MC) based depletion scheme such as the methodology used at BR2

[14]. The main features implemented to address the issues related to obtaining the power distributions at steady-state and during the transient for the tests are:

- Use of a consistent approach to model the fuel depletion, fission gamma spectrum and decay power.
- Selection of the state points at which a MCNP flux solution should be recalculated.
- Use of effective control rod positions (MWd-averaged positions) for depletion.
- Use of flux normalization factor based on the fission and capture energy specific to the 1963 BR2 core configuration.
- Automatic generation of RELAP time-dependent power distribution cards.

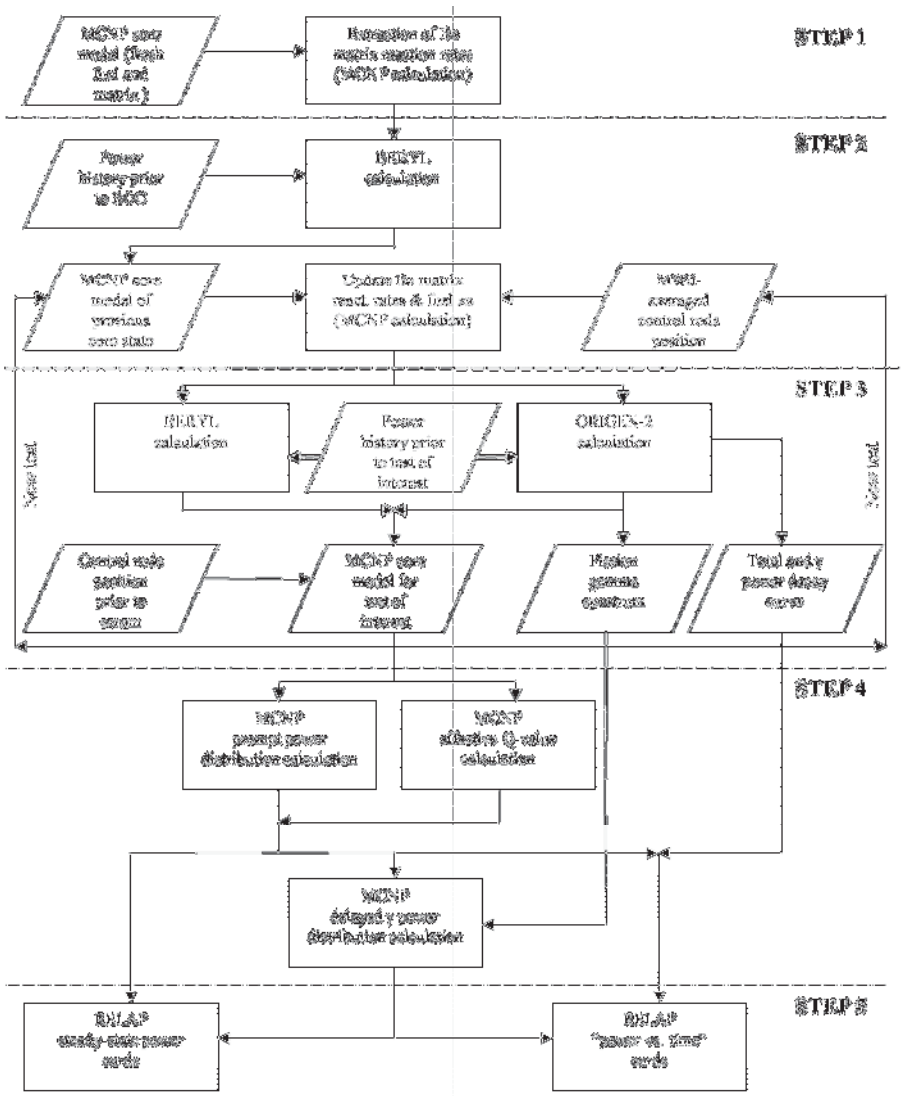

Figure 6 Current methodology flow chart

3.2.1. Determination of core state at beginning of cycle (step 1)

The dynamics of He-3, H-3 and Li-6 is such that: i) Li-6 saturates after a few hundred equivalent full power days (EFPD) [13], ii) H-3 keeps accumulating over time, iii) at steady-state, the He-3 concentration reaches an equilibrium value determined by the decay of H-3 and the capture of thermal neutrons in He-3, and iv) at reactor shutdown, He-3 starts to accumulate.

Experience at BR2 as well as previous studies [13] of reactors containing a significant amount of beryllium show that the concentrations of He-3, H-3 and Li-6 can affect significantly both the criticality of the core as well as the power distribution. The level of Be matrix poisoning is therefore a major phenomenon affecting the BR2 core state at the 1963 tests' BOC.

The BR2 SAR [15] correlates the measured He-3 reactivity impact after a day of shutdown to energy produced (related to fluence in the matrix). According to this correlation, this effect should be of the order 0.001 %dk/k per day of shutdown at the beginning of the tests and therefore negligible.

However, the Li-6 concentration has a sufficiently large impact on reactivity at BOC to necessitate its modeling. Moreover, the presence of a significant thermal absorber in the moderator will also affect the spectrum and consequently the one-group cross sections used for depletion. For generality, the evolution of all three neutron poisons (He-3, H-3 and Li-6) is modeled.

To obtain the He-3, Li-6, and H-3 concentrations at BOC, an MCNP5 model for a fresh (fuel and matrix) "configuration 4" core was used to calculate the various reaction rates needed to predict the poison concentrations using the BERYL code. This approximation is adequate since the exact core configurations from the reactor startup to BOC were similar to the "configuration 4". Since the reaction rates in Be are strongly dependant on neutron flux level and spectrum, care was taken to properly discretize the matrix based on BR2 staff recommendations. The beryllium matrix reaction rates were calculated for various zones such as beryllium hexagons surrounding FAs, beryllium hexagons surrounding control/regulating rods, control rods' Be followers, etc.

3.2.2. Evaluation of one-group cross sections and reaction rates (step 2)

To evaluate the He-3, Li-6, and H-3 concentrations, the power history before BOC [11], an average control rod (CR) position [16] and the reaction rates calculated in Step 1 are used as input data to BREYL. Using these concentrations and the MWd-averaged CR position between BOC and test A, the MCNP model is updated. This model is then used to extract reactor-specific one-group cross sections and new matrix reaction rates for Step

3. For tests occurring after test A, the MCNP5 model of the previous test is updated with the MWd-averaged CR position between the two tests.

Table 3 provides the list of uranium isotopes, actinides and fission products (FP) for which reactor-specific one-group cross sections are extracted from the MCNP5 model according to,

$$\sigma_{1g} = \frac{\int_0^{E\max} \sigma(E)\phi(E)dE}{\int_0^{E\max} \phi(E)dE} . \quad (1)$$

Table 3. Uranium, actinides and fission products cross sections extracted from MCNP.

Isotopes		
U-234	Np-238	Am-241
U-235	Np-239	Sm-150
U-236	Pu-238	Sm-151
U-238	Pu-239	Sm-152
Xe-135	Pu-240	Ru-103
Sm-149	Pu-241	Rh-103
Np-237	Pu-242	Rh-105

The BR2-specific one-group cross sections are used to replace the cross sections presents in the ORIGEN-2 standard library. Using information from the ORIGEN-2 output, it was estimated that this list of isotopes represents more than 99.9% of all absorptions in the fuel for the small burnup achieved during the tests.

3.2.3. Determination of core state at the initiation of a test (step 3)

To develop the BR2 MCNP model representing the core state at the initiation of a test, it is necessary to calculate the change in fuel and the beryllium matrix compositions due to the irradiation. IF an MCNP flux calculation was performed for each power step shown in Fig. 5, the computation time would be unpractical. Therefore, the flux solutions are obtained at the beginning and end of each of the power history color sets shown in Fig. 5.

The ORIGEN-2 depletion calculation is performed for an average FA using the one-group cross-sections from Step 2 and the appropriate detailed power history (in Fig. 5, blue power history for test A, red power history for test C and green power history for test F). Note that the cross-section burnup interpolation feature of ORIGEN-2 was turned off.

The above approach captures the main depletion effects and the overall effect of the complex Xenon dynamics resulting from the power history. Considering the small

amount of burnup achieved during the tests (about 1.0 atom % of ^{235}U at the initiation of test F), this approach is adequate since the small change in fuel burnup:

- will not significantly alter the steady-state power sharing between FAs,
- will not significantly affect the steady-state axial power distribution,
- will not require an iterative strategy to converge the number densities (no significant change the spectrum and flux level).

Moreover, it is expected that the decay power distribution is mainly a function of the steady-state power distribution (short-lived fission products) for the short duration of the transient of interest. Therefore, the approximate burnup distribution produced by this approach will have little impact on the predicted power distributions.

The ORIGEN-2 model is also used to calculate the total and gamma decay power curves as well as the fission gamma spectrum consistently with the fuel depletion. A best estimate for the steady-state power distributions requires the evaluation of the prompt and delayed components of the power (see Sections 3.2.4.1 and 3.2.4.2). In the current methodology, the predicted decay power from ORIGEN-2 is used to determine the delayed fraction of the total power at steady-state (see Eq. 4 and Table 4).

A new matrix composition (Be-9, He-3, Li-6, and H-3 number densities) is evaluated using the code BERYL, the reaction rates calculated in Step 2 and the detailed power history shown in Fig. 5.

Once new compositions are obtained, the MCNP model materials are updated. The CR positions are also updated to match the recorded positions at the initiation of the test under consideration since both the steady-state and decay power distributions depend on the instantaneous power distribution prior to scram.

3.2.4. Determination of the power distributions for a test (steps 4 and 5)

3.2.4.1. Prompt and delayed energy deposition profiles

The BR2 core heated structures, as modeled in the RELAP model [2, 17], can be arranged in the three groups shown in Fig. 7; i) the plugged group, ii) the average FA group, and iii) the instrumented group.

To calculate the steady-state power distribution for RELAP using the updated MCNP model from step 3, the two following energy deposition profiles are evaluated for the heat structures in each group:

1) A prompt energy deposition profile calculated using the f6:n and f6:p tallies in a coupled neutron-photon criticality calculation,

2) A delayed energy deposition profile using the same tallies as above in a coupled neutron-photon fixed source calculation using the decay gamma source.

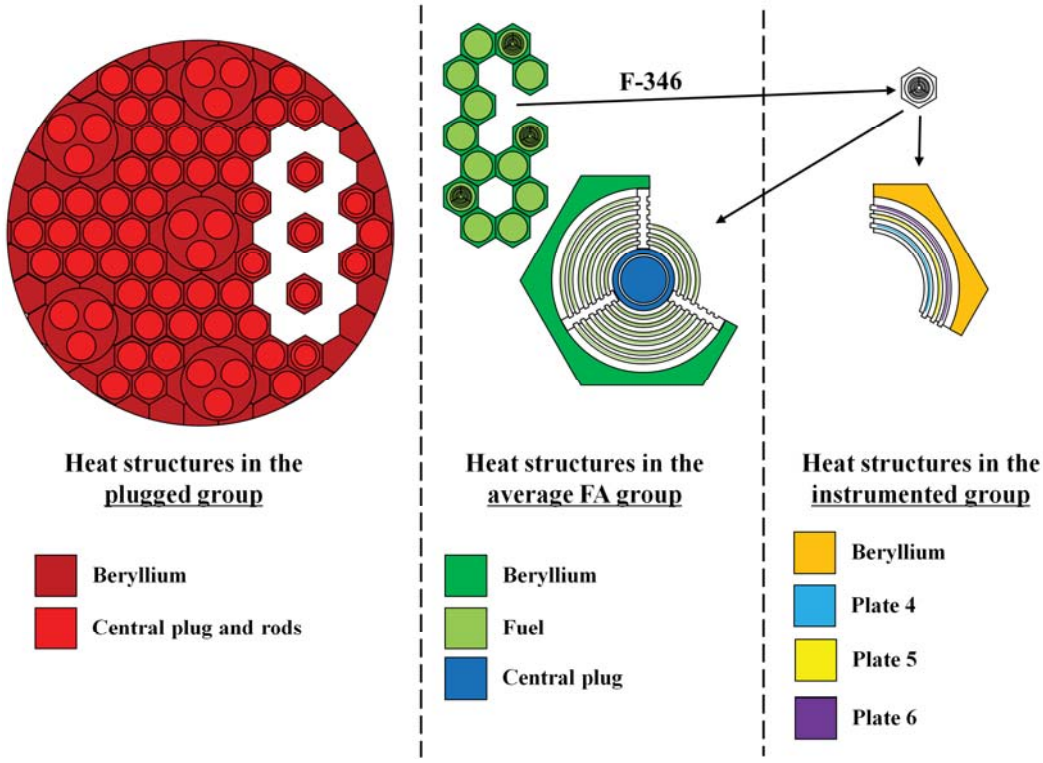

Figure 7. Heat structures considered in the RELAP model.

Note that for the instrumented FA of interest (F-346), the power was explicitly tallied for the sector containing the thermocouples in order to capture the FA sector power peaking effect due to the orientation of the FA. A sensitivity study was performed to evaluate the power azimuthal peaking within a sector for the "configuration 4" (see Section 4.6) and this effect is addressed separately in Ref. 18.

For a given power (see Section 3.2.4.2), the prompt component of the steady-state power distribution is obtain by properly normalizing the associated energy deposition profile using a reactor-specific effective recoverable energy per fission (from prompt fission and capture), i.e., an effective Q-value. This Q-value is obtained from the MCNP simulation by tallying the total energy deposited in the core per fission neutron and then applying,

$$Q_{effective}^{prompt} = E_{tally} \times \frac{\overline{\upsilon}}{k_{eff}}, \tag{2}$$

where E_{tally} is the total recoverable energy per fission neutron calculated using an f6:n,p tally, $\overline{\upsilon}$ is the average number of neutron per fission and k_{eff} is the effective neutron multiplication factor.

Since the Sylcor VIa FA has fuel enriched to 90 w/o in ^{235}U and a low burnup is achieved during the tests, the effective prompt Q-value should remain relatively constant from test

to test. However, for generality, it is recalculated every time the flux solution is recalculated.

Due to the low burnup achieved during the tests and because the axial shape remains relatively constant between the various FAs, the decay gamma source needed to obtain the delayed energy deposition profile can be approximated by:

- A multigroup gamma energy spectrum calculated by averaging the time-dependent ORIGEN-2 gamma spectrum over the duration of the transient of interest (see Section 4.3),
- A uniform spatial distribution of the gammas along the tube thickness
- An isotropic angular distribution,
- A spatial distribution S_{ijk} estimated by

$$S_{ijk} = \frac{P_i}{P_T} \cdot \frac{m_j}{m_i} \cdot \alpha_k \,, \tag{3}$$

where P_i is the neutron power (f6:n) in FA i, P_T is the total neutron power, m_j is the ^{235}U mass of plate j, and m_i is the ^{235}U mass in FA i, and α_k is an normalized average axial fission power distribution.

The delayed energy deposition profile will be normalized based on the components of the delayed power predicted by ORIGEN-2. For simplicity, this energy deposition profile is also used to evaluate the transient power distribution. Since the activation of the CR was neglected, it is expected that the CR position after scram has a negligible impact on the gamma decay power shape and therefore, using the steady-state delayed deposition profile is adequate.

3.2.4.2. Steady-state power distribution evaluation

To obtain the steady-state power distribution, it is necessary to add consistently the prompt and delayed MCNP energy deposition profiles discussed in Section 3.2.4.1. Therefore, a proper weighting factor must be obtained for each of the following contributors to the energy deposition profile: prompt neutron and gammas produced by fission and capture, delayed gamma produced by fission and delayed charged particle produced by fission.

To remain consistent with the ORIGEN-2 predicted decay power for a given test (P_{decay}^{ORIGEN}), the prompt power (P_{prompt}) used to normalized the prompt energy deposition profile is determined by

$$P_{prompt} = P_{test} - P_{decay}^{ORIGEN} = P_{test} - P_{delay}^{\gamma} - P_{delay}^{charged} \tag{4}$$

where P_{test} is the core power during a test (see Table 2), P_{decay}^{ORIGEN} is the decay power calculated from ORIGEN-2 in step 3, P_{delay}^{γ} is contribution of gammas to the decay power and $P_{delay}^{charged}$ is the contribution of charged particles to the decay power.

Equation 4 implies that external sources of heat that are part of the balance of plant, such as pump heat, have been neglected. Note that the energy released from the decay (gamma and/or beta) of isotopes created through neutron capture was not taken into account in this work.

Table 4 gives the components of the steady-state power distribution, the tallies used to calculate the energy deposition profiles and and their weighting factors.

Table 4. Components and weighting factor for steady-state power distribution.

Component	MCNP tally used for profile	Weighting factor
Prompt fission and capture	f6:n,p	P_{prompt} / P_{test}
Delayed gammas (from fission)	f6:p	$P_{delay}^{gamma} / P_{test}$
Delayed charged particles (from fission)	f6:n	$P_{delay}^{charged} / P_{test}$

The steady-state power distribution obtained by combining all the components shown in Table 4 are then used to generate the RELAP cards for each of the heat structures.

3.2.4.3. Transient power distribution

To generate the decay power distribution as a function of time after reactor scram, it is assumed that, for the period of interest (up to 60 seconds into the transient), the decay power comes mainly from the short-lived fission products whose distribution depends more on the instantaneous power than on the burnup distribution (same assumption as in the steady-state power distribution). Equations 5 and 6 are the relationships used to generate the decay power distribution for the non-fueled and fueled regions, respectively.

For each non-fueled region *i*, the normalized time-dependent power at each axial node *j* was calculated from,

$$f_{i,j} = f_{\gamma deposited\, in\, region\, i,j} \times f_{photon\, decay\, power}(t) \times [P_{core\, decay\, power}(t) / P_{steady-state}] \times 1 / f_{region\, i}, \quad (5)$$

where $f_{\gamma deposited\, in\, region\, i,j}$ is the normalized delayed gamma power in axial node *j* of region *i* (regions are shown in Fig. 7), $f_{photon\, decay\, power}(t)$ is the time-dependant fraction of the decay power produced by gammas, $P_{core\, decay\, power}(t)$ is the time-dependent core decay power as

predicted by ORIGEN-2 for a given test, $P_{steady-state}$ is the steady-state power for a given test, and $f_{region\ i}$ is the fraction of steady-state power in region *i*.

For each fueled region *i*, the normalized time-dependent power at each axial node *j* was calculated from,

$$f_{i,j} = [\ f_{\gamma deposited n region\ i,j} \times f_{photon decay power}(t) + \left(1 - f_{photon decay power}(t)\right) \times f_{\alpha\beta deposited n region\ i,j}\ ] \times \frac{P_{core decay power}(t)}{P_{steady-state} \times f_{region\ i}}, \quad (6)$$

where $f_{\alpha\beta\ deposited\ in\ region\ i,j}$ is the normalized delayed power from α and β decay (approximated by the steady-state neutron power distribution) in an axial node *j* of region *i*.

The photo-neutron contribution to the decay power is not taken into account in this methodology. This contribution should be relatively small since only slightly above 4% of the decay gammas are above the 1.666 MeV threshold [19] for the (γ, n) reaction in beryllium. This assertion is confirmed indirectly by a previous study at BR2 [20] that calculated, using point kinetics with delayed groups for neutrons and photo-neutrons, a combined decay power contribution from those two processes to be less then 0.15% of total power 20 seconds after a scram. A similar conclusion was also reached for another reactor using beryllium [21].

4. Analyses performed during development of the methodology

This section presents the analyses performed during the development of the methodology. Section 4.1 provides a comparison of the decay curves obtained using ORIGEN-2 and the ANS/ANSI-5.1-2005 standard [22]. Section 4.2 presents a study evaluating the behavior of the decay gamma spectrum during the period of interest for the test transients. Section 4.3 presents the analysis of the criticality bias for the MCNP 1963 core "configuration 4" model. Sections 4.4 and 4.5 present a verification of the computational predictions for the instrumented FA's total power as well as its axial power distribution, respectively. Section 4.6 presents the analysis of the azimuthal power peaking occurring within a sector for the 1963 core "configuration 4". Section 4.7 presents an analysis of the change in the axial power shape as a function of time during the transient.

4.1. Comparison of the ORIGEN-2 and ANS/ANSI 5.1 decay curves

As discussed in Section 3.2.3, the total and gamma decay power curves were obtained from ORIGEN-2 in order to evaluate the decay power during the transient (see Section 3.2.4). The photon data used in the ORIGEN library prior to SCALE5 [23] was shown to be adequate to calculate gamma emission and gamma heating in light-water reactor at

times longer than about one day. However, at shorter times after scram, decay heat prediction from ORIGEN-S [24, 25] was shown to be slightly lower than the ANS/ANSI-5.1-2005 standard. Therefore, a comparison of the decay heat in BR2 predicted by ORIGEN-2 and the standard was performed. Figure 8 shows a comparison of the decay curves from the ANSI/ANS-5.1-2005 standard and ORIGEN-2.

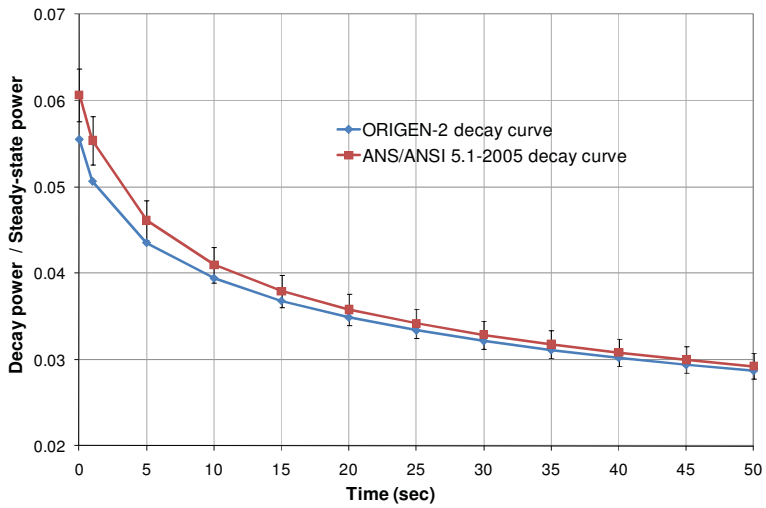

Figure 8. Decay curves calculated by ORIGEN-2 and by the ANS/ANSI 5.1 standard.

A small under-prediction can be observed in Fig. 8 for times shorter than 10 seconds after scram. However, at the time the cladding temperatures are expected to peak, i.e., at about 40 seconds after reactor scram, the two curves are in good agreement. It is also known [23] that the gamma energy spectrum from ORIGEN prior to SCALE5 under-predicts the intensity of low energy gammas for short time after reactor scram. Further studies will be performed to evaluate the impact of the gamma spectrum from ORIGEN-S "post SCALE5" on the predicted power distribution after scram.

4.2. Study of the time-dependency of the decay gamma spectrum

The analysis presented in this section is performed to justify the use of a time-averaged gamma spectrum to calculate the decay energy deposition profile in MCNP (see Section 3.2.4). Tables 5 and 6 give the contribution of each energy group, in percent, to the total gamma source as a function of time after reactor scram during test A up to 50 seconds. This data also reflects the behavior predicted by ORIGEN-2 for tests C and F.

It can be seen from these tables that for the duration of the transient of interest ORIGEN-2 predicts that the gamma spectrum will remain relatively unchanged (less than 2% change) for the energy groups contributing more than 0.2% to the total decay gamma source. Only gammas in the two highest energy groups change significantly over that period. The small contribution of these two energy groups is obvious in Fig. 9, which shows the time-averaged decay gamma spectrum predicted by ORIGEN-2.

Since the spectrum remains relatively unchanged, the time-averaged gamma energy spectrum used to calculate the gamma decay power distribution for each region is applicable. This also implies that, under these assumptions, the gamma power distribution will remain constant throughout the transient.

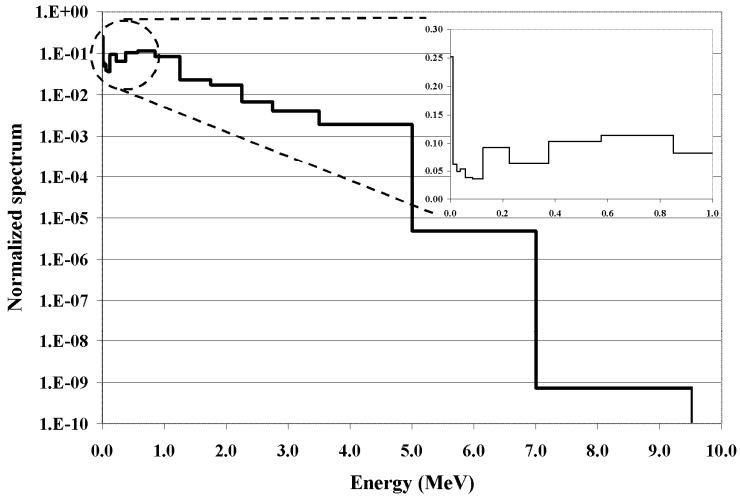

Figure 9. Time-averaged decay gamma spectrum predicted by ORIGEN-2.

Table 5. Gamma energy groups (below 1 MeV) contribution, in percent, to the decay gamma source during test A.

Time after scram (sec)	Gamma energy group midpoint (MeV)									
	0.01	0.025	0.0375	0.0575	0.085	0.125	0.225	0.375	0.575	0.85
0	26.34 %	6.38 %	4.96 %	5.71 %	4.02 %	3.76 %	9.72 %	6.12 %	9.82 %	10.61 %
1	26.21 %	6.35 %	4.96 %	5.67 %	4.00 %	3.72 %	9.65 %	6.14 %	9.90 %	10.68 %
5	25.81 %	6.27 %	4.95 %	5.54 %	3.93 %	3.65 %	9.46 %	6.22 %	10.10 %	10.96 %
10	25.46 %	6.20 %	4.93 %	5.44 %	3.86 %	3.61 %	9.33 %	6.28 %	10.23 %	11.21 %
15	25.22 %	6.15 %	4.92 %	5.37 %	3.82 %	3.58 %	9.27 %	6.33 %	10.31 %	11.39 %
20	25.04 %	6.12 %	4.92 %	5.32 %	3.79 %	3.56 %	9.23 %	6.36 %	10.37 %	11.52 %
25	24.91 %	6.09 %	4.91 %	5.28 %	3.77 %	3.54 %	9.20 %	6.38 %	10.42 %	11.63 %
30	24.80 %	6.07 %	4.91 %	5.25 %	3.75 %	3.53 %	9.17 %	6.40 %	10.47 %	11.72 %
35	24.70 %	6.05 %	4.91 %	5.22 %	3.74 %	3.52 %	9.14 %	6.41 %	10.51 %	11.80 %
40	24.61 %	6.03 %	4.91 %	5.20 %	3.72 %	3.50 %	9.11 %	6.43 %	10.55 %	11.87 %
45	24.47 %	6.01 %	4.91 %	5.16 %	3.70 %	3.49 %	9.06 %	6.45 %	10.63 %	11.99 %
50	24.35 %	5.98 %	4.90 %	5.12 %	3.68 %	3.47 %	9.01 %	6.46 %	10.70 %	12.11 %

Table 6. Gamma energy groups (above 1 MeV) contribution, in percent, to the decay gamma source during test A.

Time after scram (sec)	Gamma energy group midpoint (MeV)							
	1.25	1.75	2.25	2.75	3.5	5	7	9.5
0	7.65 %	2.13 %	1.54 %	0.63 %	0.40 %	0.22 %	1.7E-3 %	3.4E-7 %
1	7.73 %	2.16 %	1.56 %	0.64 %	0.40 %	0.22 %	1.6E-3 %	2.7E-7 %
5	7.99 %	2.22 %	1.63 %	0.66 %	0.41 %	0.21 %	9.7E-4 %	1.0E-7 %
10	8.20 %	2.27 %	1.68 %	0.67 %	0.41 %	0.20 %	4.8E-4 %	3.0E-8 %
15	8.33 %	2.30 %	1.72 %	0.68 %	0.41 %	0.20 %	2.3E-4 %	8.4E-9 %
20	8.42 %	2.32 %	1.74 %	0.69 %	0.41 %	0.19 %	1.1E-4 %	2.4E-9 %
25	8.48 %	2.33 %	1.76 %	0.69 %	0.41 %	0.19 %	5.2E-5 %	6.6E-10 %
30	8.53 %	2.34 %	1.78 %	0.69 %	0.41 %	0.18 %	2.5E-5 %	1.9E-10 %
35	8.57 %	2.35 %	1.80 %	0.70 %	0.41 %	0.18 %	1.2E-5 %	5.2E-11 %
40	8.61 %	2.36 %	1.81 %	0.70 %	0.41 %	0.18 %	5.8E-6 %	1.5E-11 %
45	8.67 %	2.37 %	1.83 %	0.70 %	0.40 %	0.17 %	1.6E-6 %	1.1E-12 %
50	8.71 %	2.38 %	1.85 %	0.71 %	0.40 %	0.17 %	5.3E-7 %	8.8E-14 %

4.3. Criticality bias of the "configuration 4" MCNP model

In order to verify that the MCNP model can be used credibly to simulate the 1963 core "configuration 4", a study of the predicted k-effective for expected critical rod positions is performed for four core states. This type of comparison provides an indication that the depletion methodology adequately models the burnup and xenon effects at the initiation of the tests.

Using the fresh (fuel and matrix) core MCNP model (see Section 3.2.1) with the control rods withdrawn to 450mm [16], a criticality bias of about +0.7% Δk/k is observed. Using the control rod height of 551mm recorded at the beginning of test A [11], the critical bias of the test A MCNP model is also about +0.7 %Δk/k from critical. Due to small inconsistencies in the exact time at which the control rod positions are recorded for tests C and F [11], the criticality bias for these tests varies between 0.6%Δk/k and 1.2%Δk/k. Even though a small increase in the criticality bias is possible for these two tests, the bias remains acceptable for all tests.

A sensitivity study performed to evaluate the impact of inserting the CR between 15-20mm from the CR positions shown in Table 2 to obtain k-effective closer to 1.0. These perturbations have a reactivity impact of about 0.8% Δk/k but had a negligible impact on FA-averages one-group cross sections (<1% change) and predicted peak cladding temperatures (about 2°C for test C).

4.4. Verification of the fuel assembly power predictions

To further verify that the MCNP5 model and methodology are adequate, the predicted FA powers was compared with experimental measurements for the four instrumented FAs shown in Fig. 3. Table 7 gives calculated FA powers for tests F and C as well as the measured FA power for similar conditions.

Table 7. Measured and calculated fuel assembly power

Fuel assembly ID	Total core power = 24MW		Total core power = 36MW	
	Measured[1] (MW)	Calculated (MW)	Measured[2] (MW)	Calculated (MW)
F-346	1.94	1.84	2.87	2.74
G-0	1.74	1.74	2.73	2.59
C-41	1.51	1.55	2.29	2.32
H-323	1.30	1.16	1.95	1.77

[1]FA powers were measured at 23.85 MW with CR positions 490 mm [8].
[2]FA powers were measured at 36.45 MW with CR positions 505 mm [8].

Considering that the reported uncertainty [8] on the measured FA power is 13% and the fact that the core states are not identical, the results given in Table 7 show a very good agreement between the measured and computed FA powers.

4.5. Comparison of axial power distributions from the current and historical approach

As an additional verification, the axial power distribution obtained with the current methodology is compared with the historical calibrated distribution (see Section 1.2). In Fig.10, it can be seen that the MCNP axial power distribution for the instrumented sector (green line) are consistent with the calibrated distribution (red line) used in the historical approach.

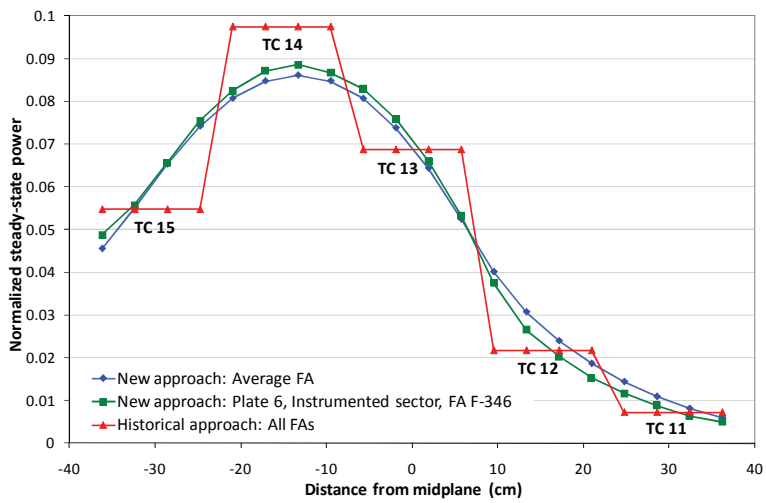

Figure 10. Current and historical axial power distributions in instrumented plate for test A

The current methodology predicts a an average power about 10%higher for TC11, TC12 and TC15 while predicting a 12% lower average power at the peak location (TC14). At the location of TC13, the discrepancy is about 1%.

4.6. Study of sector azimuthal peaking for test A

As in the current core configuration, the BR2 1963 FAs were subjected to strong azimuthal power peaking. However, in the “configuration 4”, the azimuthal peaking is produced by a different mechanism than in the current core. In the 1963 configuration, the CRs were aligned on vertical and diagonal rows (see Fig. 3) and consequently, produced a thermal neutron flux peak about the midpoint between each of the CR rows. The azimuthal power peak therefore occurred at a given location within a sector based on the orientation of the FAs with respect to that thermal neutron flux peak. The impact of two orientations of FA F-346 during test A is illustrated in Fig. 11.

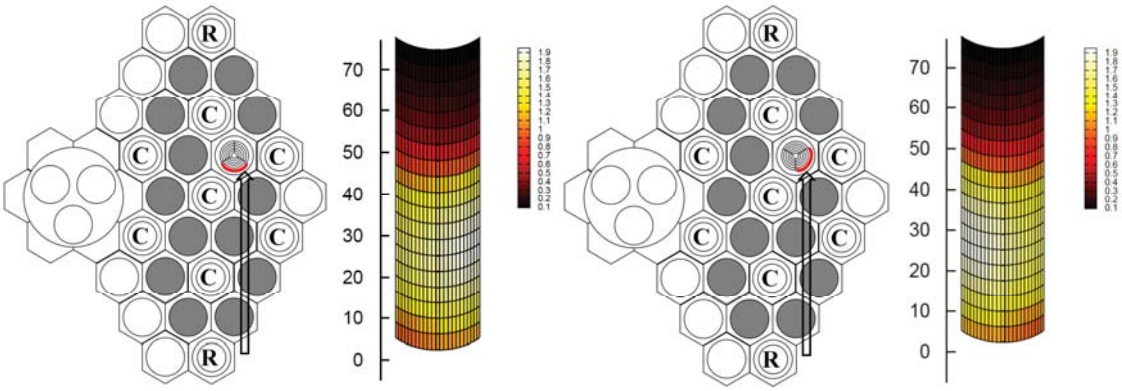

Figure 11. F-346 FA local-to-average peak for two orientations of the hot sector.

In the orientations shown in Fig. 11, thermal neutron flux peaks (and associated power peaks) occur near the aluminum stiffeners. It is expected that a power peak at that location would not result in a significant increase in cladding temperature due to the azimuthal heat conduction in the stiffener.

The worst case should therefore occur when a FA is oriented such that the thermal neutron flux peak is located near the center of a plate (sector). From a thermal-hydraulics perspective, this location of the peak is limiting since conduction to the plate's unfueled edges and the stiffeners will be minimal. Figure 12 illustrates this orientation and shows the azimuthal peaking at the axial height of the power peak (hot plane).

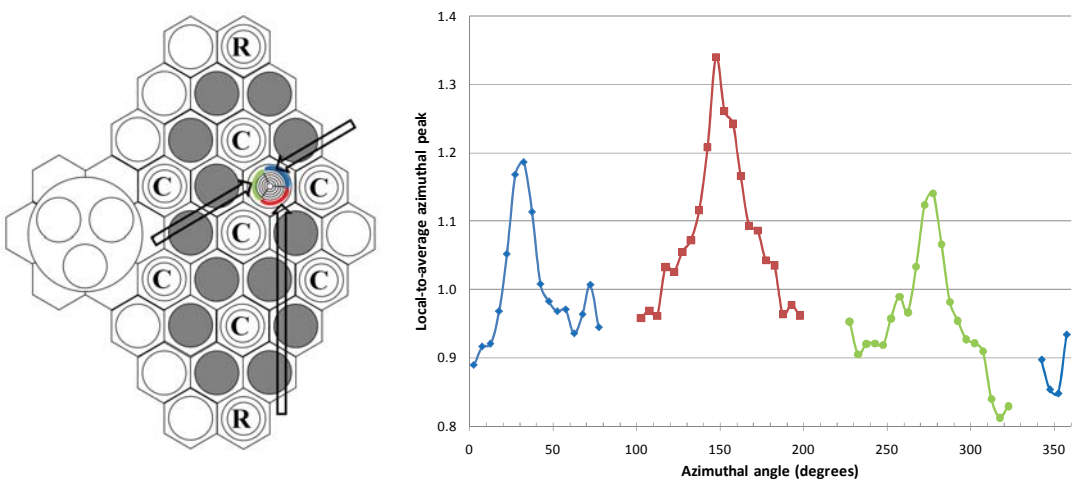

Figure 12. F-346 FA outer plate azimuthal local-to-average peak in the hot plane.

Since no accurate information regarding the orientation of the FAs during the 1963 tests is available, the analyses were performed using the sector averaged power. The impact of the azimuthal peaking is therefore studied in a separate analysis [18] using the orientation shown in Fig. 12.

4.7. Change in the axial power profile during the transient

After scram, since a larger fraction of power is generated from decay gammas, it is expected that the axial power distribution should flatten due to the relatively larger mean-free-path of gammas. Therefore, it is necessary to study the change in axial power profile during the transient in order to determine if this phenomenon must be modeled in RELAP. Figure 13 shows the ratio of the decay axial power shape to steady-state axial power shape during test C.

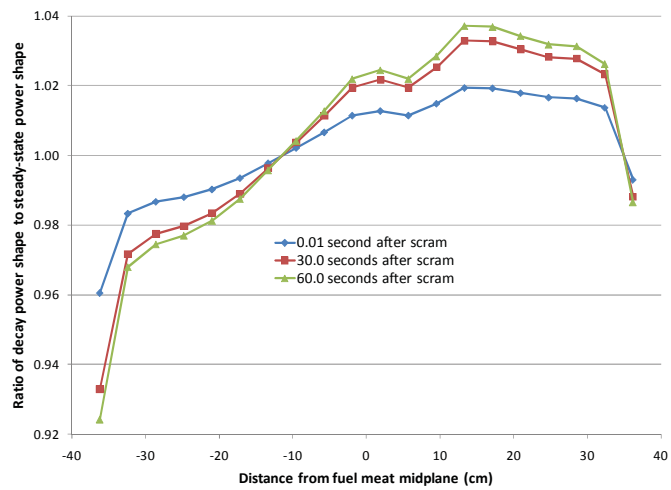

Figure 13. Ratio of the decay to steady-state axial power shapes during test C.

As expected, the axial locations with a higher steady-state power (below midplane) show a small reduction while the axial locations with a lower steady-state power show a small increase. As seen in Fig. 13, this effect is about 4%, at most, for the period of interest after reactor scram. The axial location where the power peak occurs during these tests (around 15cm below mid-plane) sees changes smaller than 1%. This effect was therefore neglected in the RELAP power distribution cards.

5. Computational results

This section presents a representative sample (from the different tests) of the computational results used to generate the RELAP steady-state and transient power cards. Section 5.1 presents a comparison of the steady-state axial power distributions in the instrumented sector obtained for the three tests. Section 5.2 presents computational results showing the steady-state power distribution among the various regions represented in the RELAP model at the initiation of test C. Section 5.3 presents a comparison of the steady-state axial power distributions obtained for the different regions of the BR2 1963 core "configuration 4". Section 5.4 shows the decay power distribution among the various regions at different times during the test F transient. Section 5.5 presents results illustrating the impact of the new best estimate methodology on peak cladding temperature during test A.

5.1. Steady-state axial power in the instrumented sector for all tests

Figure 14 presents a comparison of the steady-state axial power distributions calculated with the current methodology for the tests A, C and F.

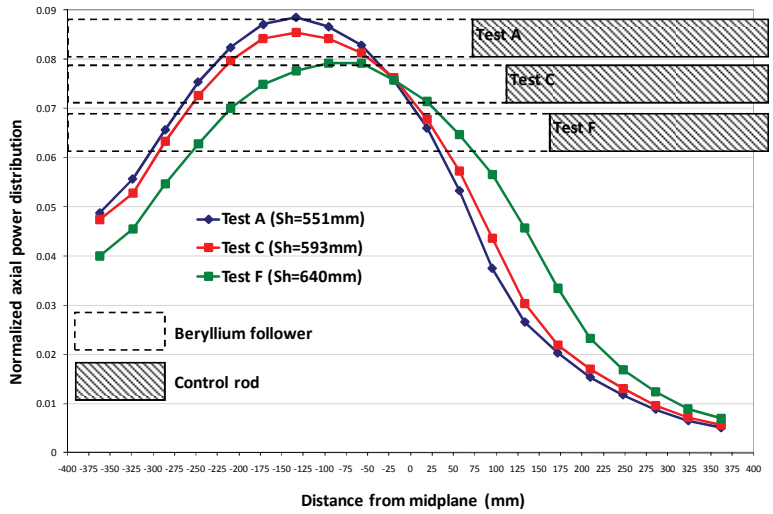

Figure 14. Axial power distributions in instrumented plate 6 for the tests A, C and F.

In can be observed that, as expected, the power distribution flattens as the CR are withdrawn further. It can also be seen that, for these three tests, the axial power peak occurs in the beryllium follower at about 20cm below the tip of the CR. These distributions are used to generate the RELAP cards specifying the steady-state axial power profile of the fuelled regions. They are also used to evaluate the axial distribution of one of the components of the decay power distribution ($f_{\alpha\beta\, deposited\, in\, region\ i,j}$ in Eq. 6).

5.2. Steady-state power fraction for each region at initiation of test C

Using the approach described in Section 3.2.4, the steady-state power for each region of the core (see Fig. 7) was calculated using MCNP. These results are used to generate the RELAP cards specifying the steady-state power in each region. Table 8 gives the percentage of total power for each region at the initiation of test C. Note that this breakdown is representative of the tests A and F.

Table 8. Percentage of steady-state power for each region at initiation of test C.

MCNP region		% of total power
RELAP channel	Heat structure	
Instrumented	F-346 - plate 4	0.45
	F-346 - plate 5	0.58
	F-346 - plate 6	0.72
	Beryllium	0.03
Average FA	Fuel	91.6
	Beryllium	1.1
	Central plug	0.29
Plugged	Beryllium	2.54
	Central plug and CRs	2.69

As expected it can be seen that, at steady-state, a large fraction of the energy is deposited in the fuel. For the 1963 core "configuration 4", this fraction is typically around 93%.

For each of the RELAP heat structures, Table 9 shows the breakdown between the power generated by neutrons and gammas at initiation of test C. Note that this breakdown is representative of the tests A and F.

Table 9. Neutron and gamma fractions of steady-state power for each region.

MCNP region		Neutron fraction	Gamma fraction
RELAP group	Heat structure		
Instrumented	FA F-346 (3 plates)	0.944	0.056
	Beryllium	0.276	0.724
	Central plug	0.041	0.959
Average FA	Fuel assemblies	0.942	0.058
	Beryllium	0.284	0.716
	Central plug	0.111	0.889
Plugged	Beryllium	0.130	0.870
	Central plug and CRs	0.046	0.954

From Table 9, it can be seen that, as expected, all non-fuelled regions are mainly heated by gammas. The percentage of power produced by gammas at steady-state varies from region to region; about 6% for a FA, about 72% for a beryllium hexagon that surround a FA, and around 90% and above for the other structures.

5.3. Steady-state axial power distributions at initiation test A

Figure 15 presents a comparison of the steady-state axial power distributions of different regions at the initiation of test A. Note that similar axial power distributions are calculated for the tests C and F.

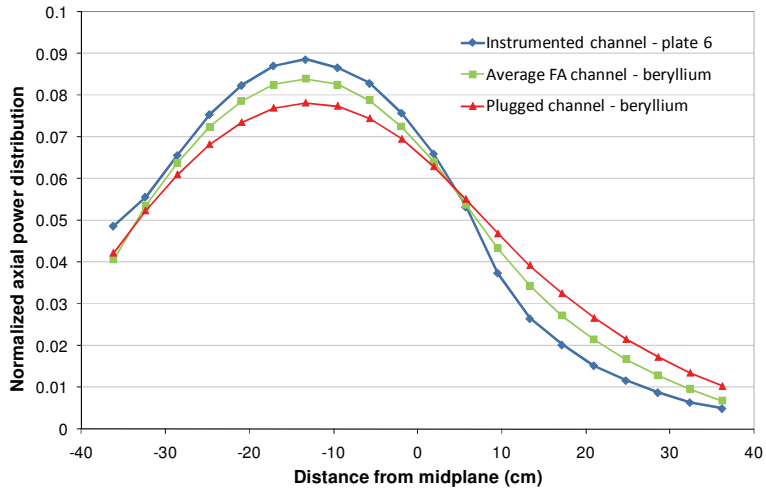

Figure 15. Steady-state axial power profiles at initiation of test A.

By comparing results in Table 9 and Fig. 15, it can be observe that regions with a larger fraction their power generated by gammas have a flatter axial profile as expected. For simplicity, the axial profiles in non-fuelled regions are reduced to five axial zones before generating the RELAP power distribution.

5.4. Decay power for each region during test F

This section presents the computational results, from test F, related to the generation of the RELAP transient power cards.

Figure 16 shows the decay heat curve (as the ratio of decay to steady-state power) generated by ORIGEN-2 for test F. Note that the decay heat curve is also representative of tests A and C.

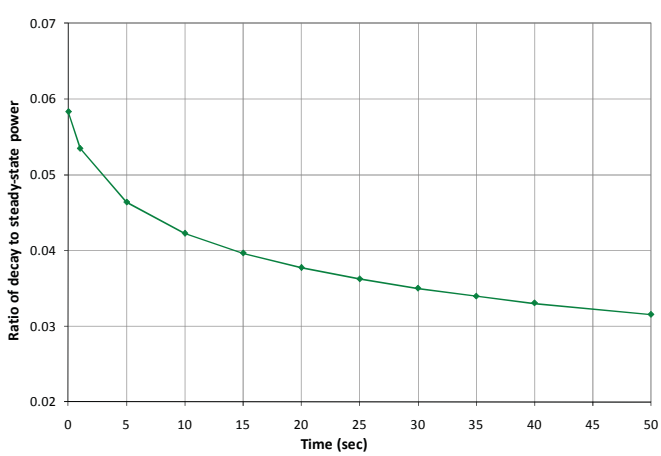

Figure 17. Decay heat curve for test F

The data shown in Fig. 16 is used to evaluate the $P_{core\,decay\,power}(t)/P_{steady-state}$ ratios in Eqs 5 and 6.

Table 10 gives the percentage of decay gamma power for each region of test F immediately after scram. Note that this breakdown is also representative of tests A and C.

Table 10. Percentage of decay gamma power for each region immediately after scram.

MCNP region		% of decay power
RELAP channel	Heat structure	
Instrumented	F-346 - plate 4	0.14
	F-346 - plate 5	0.17
	F-346 - plate 6	0.22
	Beryllium	0.62
Average FA	Fuel	26.11
	Beryllium	20.37
	Central plug	6.72
Plugged	Beryllium	30.01
	Central plug and CRs	15.64

Table 10 shows that, as expected, the decay gamma power is much more distributed among the various regions of the core than the steady-state power. For the reasons mentioned in Section 4.2, the breakdown shown in table 10 is kept constant throught the transient. This information, combined with the axial gamma power distribution, is used to evaluate $f_{\gamma deposited\,in\,region\,i,j}$ in Eqs 5 and 6.

Figure 17 shows the fraction of decay power produced by gamma as function time, $f_{photon\,decay\,power}(t)$, used in Eqs 5 and 6.

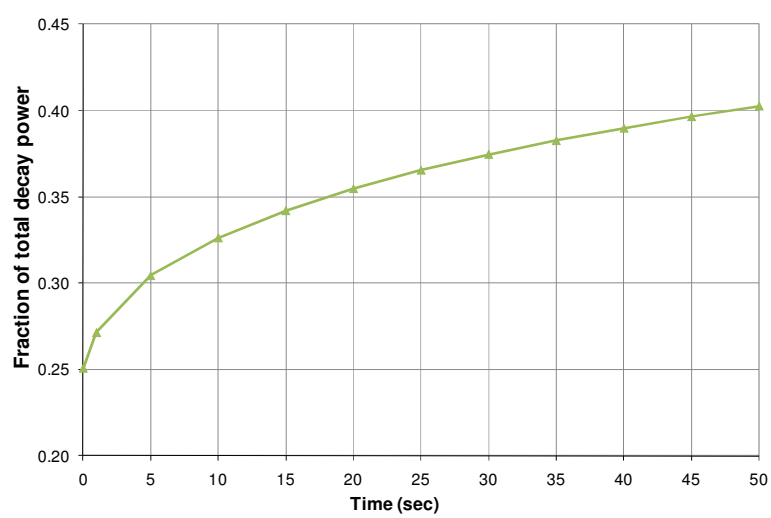

Figure 17. Fraction of decay power produced by gamma as function time

Since the fraction of the total decay power generated by gamma increases with time after scram, the total decay power tends to redistribute itself from the fuel to other regions. To illustrate this fact, the decay powers of the various regions have been combined into three zones: fuel, beryllium hexagons and other. Table 11 gives the fraction of the decay power for those three zones at steady-state and at three times during the transient. Note that this behavior is also representative of tests A and C.

Table 11. Fraction of decay power at steady-state and during the transient of test F.

Zone	Steady-state	Transient		
		0.1 s	25 s	50 s
Fuel	0.933	0.805	0.721	0.687
Be hexagons	0.026	0.119	0.170	0.190
Other	0.041	0.076	0.109	0.122

5.5. RELAP peak cladding temperature during test A

Using the steady-state and decay power distributions from both methodologies (current and historical), the cladding temperature was calculated by RELAP [17] at various heights in the instrumented fuel assembly (F-346). For the test A transient, Fig. 18 shows the measured and predicted peak cladding temperatures (TC14, 150mm below the mid-plane) with the historical and current approaches.

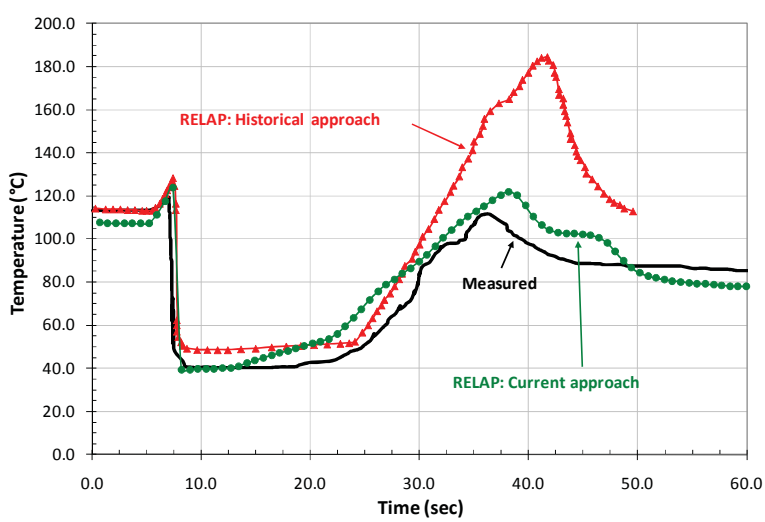

Figure 18. Peak cladding temperature (TC14) during the test A transient.

It can be observed that the power distribution obtained with the current methodology drastically improves the agreement between measured and predicted cladding temperatures.

6. Conclusions

In order to support the HEU to LEU conversion safety analyses of the BR2 reactor, RELAP simulations of a number of loss-of-flow/loss-of-pressure tests have been undertaken. Preliminary analyses showed that the conservative power distributions used historically in the BR2 RELAP model resulted in a significant overestimation of the peak cladding temperature during the transient. Therefore, it was concluded that better estimates of the steady-state and decay power distributions were needed to accurately predict the cladding temperatures measured during the tests and establish the credibility of the RELAP model and methodology.

The new approach ("best estimate" methodology) uses the MCNP5, ORIGEN-2 and BERYL codes to obtain steady-state and decay power distributions for the BR2 core during the tests A/400/1, C/600/3 and F/400/1. This methodology can be easily extended to simulate any BR2 core configuration. Comparisons with measured peak cladding temperatures showed a much better agreement when power distributions obtained with the new methodology are used.

References

[1] RELAP5-3D Code Development Team, “RELAP5-3D Code Manual,” INEEL-EXT-98-00834, 2005.

[2] Husedains, S., “Simulation of the 1963 tests for validation of the BR2 transients to be calculated by the RELAP code,” Technical note NT.56/D310063/06/SH.hq, SCK-CEN.

[3] ANSI/ANS - 5.1 - 1979, “Decay Heat Power in Light Water Reactors,” American Nuclear Society, 1979.

[4] X-5 Monte Carlo Team, “MCNP-A General Monte Carlo N-Particle Transport Code, Version 5 Volume I, II and III,” LA-UR-03-1987/LA-CP-03-0245/LA-CP-03-0284, Los Alamos National Laboratory, 2003.

[5] S. Kalcheva and E. Koonen, "Monte Carlo Evaluation of Neutron Fluences in Al Vessel of BR2: MCNP Remake of "8-configurations model"", SCK-CEN report, I-107, February 2006, BR2 Reactor, SCK-CEN, Mol, Belgium.

[6] Croff, A. G., "A User's Manual for the ORIGEN2 Computer Code," ORNL/TM-7175, July 1980.

[7] Gheeraert, F., “Composition of the core of BR02,” Research on reactor BR2 and BR02, Reference document no 1, Reactor Physics of BR02 and BR2.

[8] Stiennon, G., et al., “Etude experimentale de l’inversion de debit dans le reacteur belge BR2,” Proceedings of the Third International Conference on the Peaceful Use of Atomic Energy, Geneva, September 1964, p. 119-128.

[9] Delmas, R., et al., “Mesure des temperatures de gaine des elements combustibles du reacteur BR-2,” Journal of Nuclear Energy Parts A/B, 1965, Vol. 19, p. 501-513.

[10] Planquart et al., “Fuel assemblys in the form of concentric cylindrical plates,” Proceedings of the Third International Conference of the Peaceful Use of Atomic Energy, Gevena, September 1964.

[11] E. Koonen, BR2 reactor, unpublished information, April 2009.

[12] “Consigne Permanente de Conduite – Chapitre III,” SA/005, GEX/600/63, Groupe d’Exploitation du Reacteur BR2 et de ses Installations Connexes, Service BR2, 1963.

[13] Kulikowska, T., Andrzejewski, K., and Bretscher, M., “He-3 And Li-6 Poisoning of the Maria Reactor Beryllium Matrix,” Report IAE-40/A, Institute of Atomic Energy, 05-400 Otwock-Swierk, Poland, 1999.

[14] S.Kalcheva, E.Koonen and B.Ponsard, “Accuracy of Monte Carlo Criticality Calculations During BR2 Operation”, Nucl. Technol., 151, 201, 2005.

[15]`“Volume 4 – Veiligheidsevvalutie,” Reactor BR2 Beschrijving en veiligheidsdossier, SCK-CEN, Dossier 72. S 7680.

[16] Werz, V. R., “Messung der gemisehten Strahlungsfelder im Reaktor BR2 mit Hille von Kalorimetersonden,” Nucleonik, 6, 28-33, 1964.

[17] C. P. Tzanos and B. Dionne, “Analysis of the BR2 Loss of Flow Test A,” Nucl. Sci. and Tech., accepted for publication, 2011.

[18] C. P. Tzanos and B. Dionne, "Computational Fluid Dynamics Analyses of Lateral Heat Conduction, Coolant Azimuthal Mixing and Heat Transfer Predictions in a BR2 Fuel Assembly Geometry," ANL/RERTR/TM-11/21, Argonne National Laboratory, 2011.
[19] Wattenberg, A., "Photo-Neutron Sources and the Energy of the Photo-Neutrons," Physical Review, Volume 79, Number 8, pp. 497-507, April 1947.
[20] Beckman, A., Lenders, H., and Leonard, F., "Etude Experimental du Flux de Chaleur Maximum Admissible pour le Complexe BR2," Note technique 72.0616, 1979.
[21] B. Dionne and N. Hanan, "Impact of Photo-neutrons on transients for MURR and MITR HEU and LEU cores," Proceedings of the International Meeting on Reduced Enrichment for Research and Test Reactors, Lisbon, Portugal, October 10-14, 2010, 12 pages.
[22] ANSI/ANS - 5.1 - 2005, "Decay Heat Power in Light Water Reactors," American Nuclear Society, 2005.
[23] Gauld, Ian, "Validation of ORIGEN-S Decay Heat Predictions for LOCA Analysis," Proceedings of the ANS Topical Meeting on Reactor Physics PHYSOR-2006, Vancouver, Canada, 2006.
[24] Gauld, I. C. and Murphy, B. D., "Updates to the ORIGEN-S Data Libraries Using ENDF/B-VI, FENDL-2.0, and EAF-99 Data," ORNL/TM-2003/118, Oak Ridge National Laboratory, Oak Ridge, TN, 2004.
[25] Parks, C. V., "Overview of ORIGEN2 and ORIGEN-S: Capabilities and Limitations," 1992 International High-Level Radioactive Waste Management Conference, Las Vegas, Nevada, USA, 1992.

Nuclear Engineering Division
Argonne National Laboratory
9700 South Cass Avenue, Bldg. 208
Argonne, IL 60439-4842

www.anl.gov

Argonne National Laboratory is a U.S. Department of Energy
laboratory managed by UChicago Argonne, LLC